

# Asymmetries of azimuthal photon distributions in non-linear Compton scattering in ultra-short intense laser pulses

D. Seipt\* and B. Kämpfer

*Helmholtz-Zentrum Dresden-Rossendorf,*

*P.O. Box 510119, 01314 Dresden, Germany and*

*TU Dresden, Institut für Theoretische Physik, 01062 Dresden, Germany*

(Dated: October 30, 2018)

## Abstract

Non-linear Compton scattering in ultra-short intense laser pulses is discussed with the focus on angular distributions of the emitted photon energy. This is an observable which is accessible easily experimentally. Asymmetries of the azimuthal distributions are predicted for both linear and circular polarization. We present a systematic survey of the influence of the laser intensity, the carrier envelope phase and the laser polarization on the emission spectra for single-cycle and few-cycle laser pulses. For linear polarization, the dominant direction of the emission changes from a perpendicular pattern with respect to the laser polarization at low-intensity to a dominantly parallel emission for high-intensity laser pulses.

PACS numbers: 12.20.Ds, 32.80.Wr, 41.60.-m

Keywords: ultra-short laser pulses, non-linear Compton, azimuthal spectrum, asymmetry

---

\*Electronic address: d.seipt@hzdr.de; Present address: Helmholtz-Institute Jena, Friedrich Schiller Universität Jena, 07743 Jena, Germany

## I. INTRODUCTION

The development of novel bright short-pulsed X-ray radiation sources is an important issue with respect to applications in materials research, dynamics investigations and biological structure ranging up to medical application [1]. At the heart of these table-top X-ray sources is the inverse Compton process, where optical laser photons are scattered off relativistic electrons, possibly laser accelerated ones [2], and Doppler up-shifted to the X-ray regime. While quasi-monochromatic X-rays may be achieved using long laser pulses at rather low intensities, pulsed broadband X-ray sources can be developed with high-intensity short pulse lasers, on the contrary. Besides the application-oriented research, the laser-particle interaction offers a rich variety of interesting perspectives also for fundamental physics of particle dynamics and radiation processes in strong electromagnetic fields, both experimentally and theoretically [3]. For instance, the formation of QED avalanches at ultra-high laser intensities is related to the emission of high-energy photons off ultra-relativistic electrons and subsequent pair production induced by those very photons [4, 5].

Here, we focus on the non-linear Compton scattering process, where photons from an intense laser pulse ( $L$ ) scatter off a relativistic free electron ( $e$ ), emitting a single non-laser photon  $\gamma'$  in the reaction  $e + L \rightarrow e' + \gamma' + L$ . Multi-photon interactions due to the large photon density in the laser pulse give rise to non-linear effects such as the emission of high harmonics and the intensity-dependent red-shift of the scattered radiation [3]. Each of the harmonics shows a characteristic multi-pole pattern, which in fact was used for an experimental identification of the higher harmonics [6, 7]. Non-linear strong-field effects for Compton scattering, and also for the related process of pair production, have been observed in the SLAC E-144 experiment [8, 9]. The detailed theoretical and experimental knowledge of the radiation spectra might allow to use the emitted photon radiation as a diagnostics tool to measure, e.g., the laser intensity [10], or to determine the carrier envelope phase of the laser pulse [11], or the parameters of the electron beam [12].

The theoretical investigations of non-linear Compton scattering started shortly after the invention of the laser in a series of seminal papers [13–19] (see also [20] for a complete overview of the literature as well as the reviews [3, 21]). While these early papers paved the way for further investigations, they mostly specified monochromatic infinite plane waves to model the laser field since at that time long picosecond and nanosecond laser pulses

were common. However, nowadays the use of ultra-short, femtosecond laser pulses has become standard due to the development of chirped pulse amplification which allows to reach new high-intensity frontiers with lasers such as ELI [22] envisaging intensities as high as  $10^{24}$  W/cm<sup>2</sup> in pulses of 15 fs. Even shorter pulse lengths will become available with the petawatt field synthesizer (PFS) [23], producing high intensities with pulse lengths of the order of 5 fs, which corresponds to less than two laser cycles.

In such short laser pulses, the Compton spectra are drastically altered [24–28] as compared to the previously common treatment by means of infinitely long plane waves. Important effects are the ponderomotive broadening of the harmonics and the appearance of substructures, anisotropies in the angular spectra as well as the relevance of the carrier envelope phase [29, 30]. For instance, it has been shown that the value of the carrier envelope phase determines the angular region of emission [11]. Due to the large bandwidth of the emitted radiation it is in general not possible to distinguish individual harmonics in strong pulsed fields. Therefore, in this paper, we discuss energy-integrated angular spectra in ultra-short intense laser pulses. We give a systematic survey of the influence of the laser pulse parameters on the angular spectra, focussing on asymmetries in azimuthal distributions of the emitted energy.

Our paper is organised as follows: After a concise presentation of the Volkov states and the basic framework, we derive the analytical expressions for the differential emission probability and energy distribution in Section II. In Section III, we present a comprehensive numerical study of the azimuthal spectra in ultra-short laser pulses and the dependence of the photon energy distributions on the laser pulse parameters. In Section IV we discuss the total amount of emitted energy in relation to the primary energy flux in the laser pulse. The conclusions are drawn in Section V. In Appendix A we briefly discuss the classical framework, that is Thomson scattering, for the angular photon spectra. We find that the total emitted energy is proportional to the integrated primary energy flux in the laser pulse. In Appendix B, we derive the non-relativistic and ultra-relativistic limits the azimuthal cross sections for Compton scattering of a polarized photon in perturbative QED. It is shown that, in the ultra-relativistic case, the emission is azimuthally symmetric in the leading order.

## II. SCATTERING AMPLITUDE, PROBABILITY AND EMITTED ENERGY

To account for the strong laser pulse non-perturbatively, one can work within the Furry picture and employ Volkov wavefunctions as a basis for the perturbative expansion of the  $S$  matrix. The Volkov states [31] are solutions of the Dirac equation in the presence of the plane-wave background field<sup>1</sup>  $A_\mu$

$$(i\cancel{\partial} - e\cancel{A}(\phi) - m)\Psi(x) = 0. \quad (1)$$

We consider here a laser pulse described by the transverse ( $A \cdot k \equiv A_\mu k^\mu = 0$ ) vector potential

$$A^\mu(\phi) = A_0 g(\phi) \text{Re}(\epsilon_\pm^\mu e^{-i(\phi + \phi_{\text{CE}})}), \quad (2)$$

depending on the invariant phase  $\phi = k \cdot x$  with the laser wave four-vector  $k^\mu = (\omega, 0, 0, -\omega)$ . The polarization of the background field is described by complex polarization vectors  $\epsilon_\pm^\mu = \delta_1^\mu \cos \xi \pm i\delta_2^\mu \sin \xi$  (the quantity  $\delta_\nu^\mu$  denotes the Kronecker symbol), with polarization parameter  $\xi$ . Here,  $\xi = 0, \pi/2$  means linear polarization and  $\xi = \pi/4$  denotes circular polarization; all other values refer to an arbitrary elliptic polarization. In (2),  $g(\phi)$  denotes the pulse envelope. The limit  $g \rightarrow 1$  refers to infinitely long plane wave fields (IPW), while a finite support of  $g(\phi)$  describes a pulsed plane wave (PPW) to be specified below. The relative phase between the pulse envelope and the carrier wave is the carrier envelope phase (CEP)  $\phi_{\text{CE}}$ . The dimensionless laser amplitude  $a_0$ , which quantifies relativistic and multi-photon effects, is defined as  $a_0 = |e|A_0/m$ , where  $A_0$  denotes the amplitude of the vector potential (2), and  $e = -|e| = -\sqrt{4\pi\alpha}$  is the charge of the electron with the fine structure constant  $\alpha \simeq 1/137$ . The values of  $a_0$  are related to the peak laser intensity  $I$  and the laser central wavelength  $\lambda$  via  $a_0^2 = 7.3 \times 10^{-19} I[\text{W}/\text{cm}^2]\lambda^2[\mu\text{m}]$ .

The solutions of Eq. (1) are given by [32]

$$\Psi_{pr}(x) = \left(1 + \frac{e}{2k \cdot p} \cancel{k} \cancel{A}\right) \exp \left\{ -ip \cdot x - \frac{i}{2k \cdot p} \int_0^\phi d\phi' (2ep \cdot A - e^2 A \cdot A) \right\} u_p, \quad (3)$$

with the free spinor  $u_{pr}$ , normalized to  $\bar{u}_{pr} u_{pr'} = 2m\delta_{rr'}$ .

---

<sup>1</sup> Natural units with  $\hbar = c = 1$  are employed throughout this paper, as well as the Feynman dagger notation  $\cancel{\not{p}} = \gamma_\mu p^\mu$ .

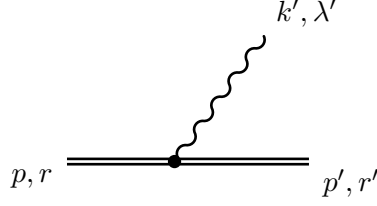


FIG. 1: First-order Feynman diagram for non-linear one-photon Compton scattering within the Furry picture. In strong-field QED, the one-photon Compton scattering appears as the decay of a laser dressed Volkov electron state (straight double lines) with momentum  $p$  and spin quantum number  $r$  into another laser dressed electron with momentum  $p'$  and spin  $r'$  while emitting a photon (wavy line) with momentum  $k'$  in a polarization state  $\lambda'$ .

The Volkov states Eq. (3), which include the interaction of the laser pulse with the electrons, are used as in- and out-states for the electrons when calculating matrix elements. The interaction with non-laser photons is treated in perturbation theory, depicted in the Feynman diagram in Fig. 1 for non-linear Compton scattering in a strong laser field, i.e. the emission of a non-laser mode photon off a Volkov electron. Thus, non-linear Compton scattering is a first-order process “above” the non-perturbative interaction of the electron with the laser field. The  $S$  matrix for the process is obtained by using the corresponding Feynman rules [33] as

$$S = -ie \int d^4x \bar{\Psi}_{p'r'}(x) \not{\epsilon}'_{\lambda'} e^{ik' \cdot x} \Psi_{pr}(x). \quad (4)$$

Performing the spatial integrations over the light-front variables<sup>2</sup>  $\mathbf{x}^\perp$  and  $x^-$  one arrives at

$$S = -ie(2\pi)^4 \int \frac{ds}{2\pi} \delta^{(4)}(p' + k' - p - sk) \mathcal{M}(s), \quad (5)$$

$$\mathcal{M}(s) = T_0 \mathcal{C}_0(s) + T_+ \mathcal{C}_+(s) + T_- \mathcal{C}_-(s) + T_2 \mathcal{C}_2(s) \quad (6)$$

with Dirac current structures

$$T_0 = \bar{u}_{p'r'} \not{\epsilon}' u_{pr}, \quad (7)$$

$$T_\pm = \bar{u}_{p'r'} (d_{p'} \not{\epsilon}'_\pm \not{k} \not{\epsilon}' + d_p \not{\epsilon}' \not{k} \not{\epsilon}'_\pm) u_{pr}, \quad (8)$$

$$T_2 = d_p d_{p'} (\epsilon' \cdot k) \bar{u}_{p'r'} \not{k} u_{pr}, \quad (9)$$

<sup>2</sup> The light-front components of a four-vector  $x^\mu$  are defined as  $x^\pm = x^0 \pm x^3$  and  $\mathbf{x}^\perp = (x^1, x^2)$  with the scalar product  $x \cdot y = (x^+ y^- + x^- y^+)/2 - \mathbf{x}^\perp \cdot \mathbf{y}^\perp$ . The four-dimensional volume element reads  $d^4x = dx^+ dx^- d^2\mathbf{x}_\perp/2$ . Note that  $k^- = 2\omega$  is the only non-vanishing light-front component of the laser four-vector  $k^\mu$  and, therefore,  $\phi = \omega x^+$ .

and  $d_{p^{(\prime)}} = ma_0/(2k \cdot p^{(\prime)})$ . The variable  $s$  in (5) parametrizes the momentum transfer between the background laser field and the electron by means of the momentum conservation  $p + sk = p' + k'$ . It might be interpreted as net number of laser photons absorbed by the electron only in the IPW case due to the periodicity of the background field which allows to interpret the discrete Fourier components of the classical background field as “quanta” with momentum  $k^\mu$ . Thus, in the IPW case the energy resolved photon spectrum consists of discrete harmonics, while in the PPW case a smooth continuous spectrum emerges.

Evaluating the integral over  $s$  in (5) fixes the value  $s \equiv (k' \cdot p)/(k \cdot p')$  as a function of the frequency and polar angle of the emitted photon. This equation may be inverted to yield

$$\omega'(s, \vartheta) = \frac{sk \cdot p}{(p + sk) \cdot n'} = \frac{s\omega e^{2\zeta}}{1 + e^\zeta \sinh \zeta (1 - \cos \vartheta) + s \frac{\omega e^\zeta}{m} (1 + \cos \vartheta)} \quad (10)$$

with  $n' = (1, \mathbf{n}')$ , the unit vector  $\mathbf{n}' = (\sin \vartheta \cos \varphi, \sin \vartheta \sin \varphi, \cos \vartheta)$ , i.e.  $k' = \omega' n'$ , and the initial electron rapidity  $\zeta = \text{Arcosh } \gamma$ . The energy-momentum conservation is reduced to the conservation of three light-front components of momentum,  $p^+ = p'^+ + k'^+$  and  $\mathbf{p}_\perp = \mathbf{p}'_\perp + \mathbf{k}'_\perp$ . The integrals over the laser phase determining the amplitude of the process are given by

$$\left\{ \begin{array}{l} \mathcal{C}_0(s) \\ \mathcal{C}_\pm(s) \\ \mathcal{C}_2(s) \end{array} \right\} = \int_{-\infty}^{\infty} d\phi e^{is\phi - if(\phi)} \left\{ \begin{array}{l} 1 \\ g(\phi) e^{\mp i(\phi + \phi_{\text{CE}})} \\ g^2(\phi) (1 + \cos 2\xi \cos 2(\phi + \phi_{\text{CE}})) \end{array} \right\} \quad (11)$$

with

$$f(\phi) = \int_0^\phi d\phi' \left\{ g(\phi') \text{Re} \left[ \alpha_+ e^{-i(\phi' + \phi_{\text{CE}})} \right] + \beta g(\phi')^2 [1 + \cos 2\xi \cos 2(\phi' + \phi_{\text{CE}})] \right\} \quad (12)$$

and the coefficients  $\alpha_+ = d_p(2\epsilon_+ \cdot p) - d_{p'}(2\epsilon_+ \cdot p')$  and  $\beta = d_p^2(k \cdot p) - d_{p'}^2(k \cdot p')$ . The integral  $\mathcal{C}_0(s)$  needs special a treatment as it is an integral over an infinite interval for a pure phase factor due to the lacking pre-exponential pulse envelope function  $g(\phi)$ . It contains contributions from the free electron motion outside the laser pulse leading to a divergent contribution at zero momentum transfer  $s = 0$ . For  $s > 0$ ,  $\mathcal{C}_0$  can be related to the well defined integrals  $\mathcal{C}_\pm$  and  $\mathcal{C}_2$  — which are rendered finite by the appearance of the pre-exponential pulse shape functions — by the principle of gauge invariance [34, 35]

$$s\mathcal{C}_0(s) = \frac{\alpha_+}{2} \mathcal{C}_+(s) + \frac{\alpha_-}{2} \mathcal{C}_-(s) + \beta \mathcal{C}_2(s). \quad (13)$$

The differential emission probability, depending on momentum as well as spin and polarization variables of the out-states, reads  $dW_{rr'\lambda'} = |S|^2 d\Pi / (2p^+)$  with the Lorentz invariant phase space element

$$d\Pi = \frac{d^3k'}{(2\pi)^3 2\omega'} \frac{d^2\mathbf{p}'_{\perp} dp'^+}{(2\pi)^3 2p'^+}, \quad (14)$$

where the final electron phase space is conveniently parametrized in terms of light-front variables due to the light-front momentum conservation. Integrating over the final-electron variables with the momentum conservation in Eq. (5) one gets

$$dW_{rr'\lambda'} = \frac{\alpha\omega' |\mathcal{M}(s(\omega'))|^2}{16\pi^2 k \cdot p k \cdot p'} d\omega' d\Omega, \quad (15)$$

where  $d\Omega = d\varphi d\cos\vartheta$  is the solid angle element related to the emitted photon of energy  $\omega'$ . For numerical calculations, it is more convenient to employ  $s$  as the independent variable, instead of  $\omega'$ , since then the three phase space integrals are independent from each other. The transformation of the differentials reads  $d\omega' = \frac{\omega'}{s} \frac{k \cdot p'}{k \cdot p} ds$  and the phase space of the emitted photon is characterized by  $\varphi \in [-\pi, \pi)$ ,  $\vartheta \in [0, \pi]$  and  $s \in (0, \infty)$ .

We are not interested in the spin and polarization states, so we average over the initial spin  $r$  and sum over the final state spin and polarization variables, thus obtaining the differential probability

$$\begin{aligned} w(s, \vartheta, \varphi) &\equiv \frac{1}{2} \sum_{r, r', \lambda'} \frac{dW_{rr'\lambda'}}{ds d\Omega} \\ &= \frac{\alpha m^2 \omega'^2}{8\pi^2 (k \cdot p)^2 s} \left\{ -2|\mathcal{C}_0|^2 + \frac{a_0^2}{2} \left( 1 + \frac{u^2}{2(1+u)} \right) \right. \\ &\quad \left. \times \left[ |\mathcal{C}_+|^2 + |\mathcal{C}_-|^2 + \cos 2\xi (\mathcal{C}_+ \mathcal{C}_-^* + \mathcal{C}_- \mathcal{C}_+^*) - \mathcal{C}_0 \mathcal{C}_2^* - \mathcal{C}_2 \mathcal{C}_0^* \right] \right\} \end{aligned} \quad (16)$$

with the invariant variable  $u = (k \cdot k') / (k \cdot p')$ . In this expression, the azimuthal angle  $\varphi$  appears solely via the non-linear exponentials  $f(\phi)$  of the functions  $\mathcal{C}_n$  defined in (11).

The energy  $E$  of the emitted radiation is given by the time component of the momentum four-vector  $P^\mu$  of the radiation field

$$P^\mu = \int ds d\Omega k'^\mu w(s, \vartheta, \varphi). \quad (18)$$

Note that the emitted energy  $E$  and also the corresponding azimuthal distribution  $dE/d\varphi$  are not Lorentz invariant. Instead,  $E$  transforms under Lorentz boosts as the time component

of the four-vector  $P^\mu$ ,  $\bar{E} = \hat{\gamma}(E + \hat{\mathbf{v}} \cdot \mathbf{P})$ , where  $\hat{\mathbf{v}}$  is the relative velocity and  $\hat{\gamma} = (1 - \hat{\mathbf{v}}^2)^{-1/2}$  is the corresponding Lorentz factor. On the contrary, the total probability

$$W = \int ds d\Omega w(s, \vartheta, \varphi) \quad (19)$$

is a Lorentz invariant quantity.

### III. NUMERICAL ANALYSIS

We focus on parameters which are accessible in various laboratories. To be specific, one parameter set which may allow for an experimental verification refers to an operating set-up at the Helmholtz-Zentrum Dresden-Rossendorf (HZDR) using the electron linear accelerator ELBE [36] in combination with the short-pulse high-intensity laser DRACO [37]. For the following numerical survey we specify head-on collisions of an optical laser pulse ( $\omega = 1.55$  eV) with an electron beam which has an energy corresponding to  $\gamma = 100$ .

For weak laser fields,  $a_0 \ll 1$ , the emission is dominantly into a narrow cone with a typical opening angle  $\vartheta_{\text{cone}} \sim 1/\gamma$ , centred at the initial velocity  $\mathbf{u}_0$ . For larger laser strength  $a_0 > 1$ , the radiation cone widens due to the intensity dependent radiation pressure with a typical angle  $\vartheta_{\text{cone}} \sim a_0/\gamma$ . In particular, for a laser intensity of  $a_0 = 2\gamma$  the mean emission angle is  $\vartheta_{\text{cone}} = \pi/2$  [20].

In the following, we use the pulse envelope function

$$g(\phi) = \begin{cases} \cos^2\left(\frac{\phi}{2N}\right) & \text{for } \phi \in [-\pi N, \pi N], \\ 0 & \text{elsewhere,} \end{cases} \quad (20)$$

introduced in Eq. (2) and entering the coefficient functions  $\mathcal{C}_n$ , with compact support on the interval  $[-\pi N, \pi N]$ . The number of optical cycles of the laser pulse is  $N$ .

#### A. Double differential angular distribution

We start our analysis by discussing the double differential energy distribution

$$\frac{dE}{d\Omega} = \int_0^\infty ds \omega'(s, \vartheta) w(s, \vartheta, \varphi). \quad (21)$$



We have in mind a high-granular pixel photon detector placed in the radiation cone that allows to measure angularly resolved energy-integrated spectra. The quantity (21), as energy-integrated emitted energy, does not suffer from the possible problem of detector pile-ups, where two individual photons are detected as a single photon of summed energy. Such false detections may happen if the incident photon flux is too large for the temporal resolution of the detector. It provides, thus, an easily observable quantity to characterize appropriately the Compton spectrum. The angular resolution can be improved by increasing the distance of the detector from the interaction point of the electron beam and the laser pulse.

Figure 2 exhibits a series of the distributions  $dE/d\Omega$  as contour plots. At low laser intensity,  $a_0 \ll 1$ , the shape of the distribution is oriented perpendicularly to the polarization vector, which is  $\mathbf{e}_x$  in our case. This is the usual dipole-type emission. For increasing values of  $a_0 > 1$ , the shape of the spectrum flips and is oriented in the direction of the polarization vector. This transition is characteristic for the non-linear interactions. The details of the spectra for field strengths  $a_0 > 1$ , i.e. whether it is an unidirectional emission as in the central panel of Fig. 2 or a bi-polar emission in the direction of the laser polarization, depends strongly on further pulse parameters. For ultra-short pulses this is mainly dominated by the value of the CEP. These details are studied in the next subsection using the azimuthal distributions.

In the right panel of Fig. 2, the corresponding angular distribution is exhibited for a circularly polarized laser pulse with  $a_0 = 3$ . Also in this case, strong asymmetries arise. The distribution peaks in the direction where the laser vector potential (depicted as black curve) reaches its maximum value and almost vanishes in the opposite direction. The assertion of the radiation having an opening angle  $\sim a_0/\gamma$  for  $a_0 > 1$  is clearly verified by the angular distributions in Fig. 2.

## B. Azimuthal distributions

The information on the angular distribution of the emitted energy can be condensed into the azimuthal distribution by integrating over the polar angle via

$$\frac{dE}{d\varphi} = \int_0^\infty ds \int_0^\pi d\vartheta \sin\vartheta \omega'(s, \vartheta) w(s, \vartheta, \varphi). \quad (22)$$

For long pulses and IPW laser fields, the azimuthal spectra show a characteristic multi-pole

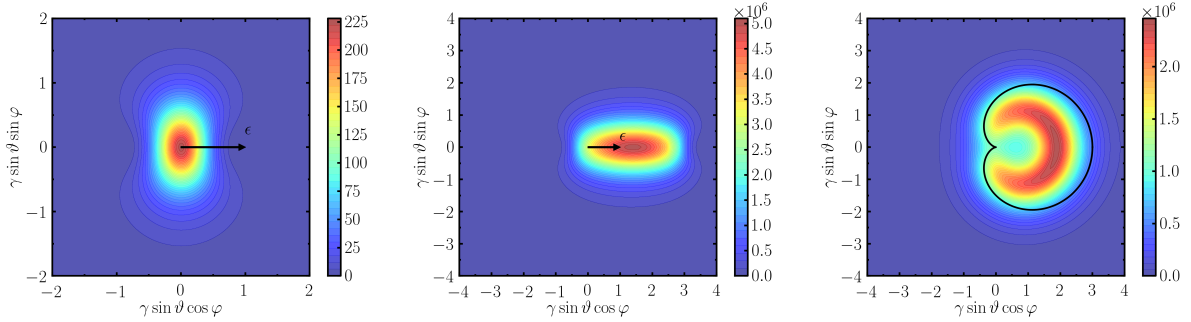


FIG. 2: Double differential angular photon energy distribution  $dE/d\Omega$  for a single-cycle ( $N = 1$ ) linearly polarized laser pulse with  $\phi_{\text{CE}} = 0$  for  $a_0 = 0.01$  (left panel) and  $a_0 = 3$  (center panel). The arrows denote the direction of the linear laser polarization vector  $\epsilon$ . In the right panel, the result for circular polarization is shown for  $a_0 = 3$ . In that case, the black curve depicts the amplitude of the laser vector potential in the  $x - y$  plane.

pattern for each harmonic, which have been observed by choosing a single harmonic using appropriate energy filters [6, 7]. In the case of a short intense laser pulse, the distinction of different harmonics is not possible. We thus study, as in the previous subsection, the energy-integrated spectrum. In the following, the azimuthal distribution  $dE/d\varphi$  of the emitted energy will be analysed systematically.

### 1. Dependence on the laser intensity

The differential azimuthal energy spectra  $dE/d\varphi$  are exhibited in Fig. 3 for a pulse length  $N = 1$ , i.e. for a single-cycle laser pulse. At low laser intensity,  $a_0 = 0.01$  (left panel), the emission has a strong dipole pattern with the preferred emission in the plane transverse to the polarization of the laser, which is here chosen as the  $x$  axis, i.e.  $\varphi \sim 0^\circ, 180^\circ$ . Upon increasing the laser strength up to  $a_0 = 1$  and  $a_0 = 3$  (middle and right polar diagrams), the shape of the spectrum develops towards an unidirectional emission in the direction of the laser polarization. The azimuthal spectra show the same qualitative behaviour as the double differential angular distributions discussed above. This is explained by the behaviour of the vector potential, depicted in the rightmost panel of Fig. 3, which has a strong asymmetry and acquires large values only in the direction  $\varphi = 0$ . The typical range of values for the variable  $s$  scales as  $a_0^3$  [32], as depicted in Fig. 4. However, due to the large asymmetry

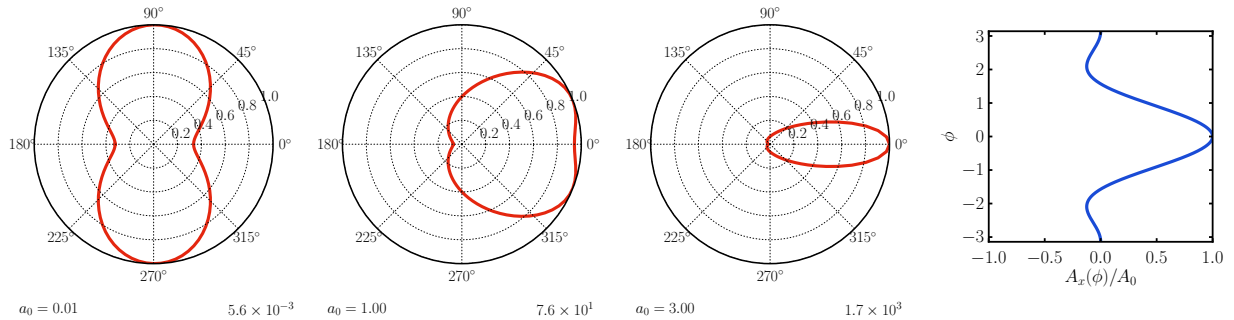


FIG. 3: The normalized azimuthal distributions of emitted energy  $dE/d\varphi$  for non-linear Compton scattering as a function of the azimuthal angle  $\varphi$  in a single-cycle laser pulse with  $N = 1$  and  $\phi_{\text{CE}} = 0$  for linear polarization ( $\xi = 0$ ) for various values of  $a_0 = 0.01, 1$  and  $3$  (from left to right). In the rightmost panel, the laser vector potential  $A^\mu$  is plotted as a function of the laser phase  $\phi$  (note the inverted axes). The labels at each panel give the maximum values of  $dE/d\varphi$  in units of eV. The calculations have been performed in the laboratory frame where the angle  $\vartheta$  was integrated over a cone with opening angle  $3/\gamma$  around the initial electron momentum.

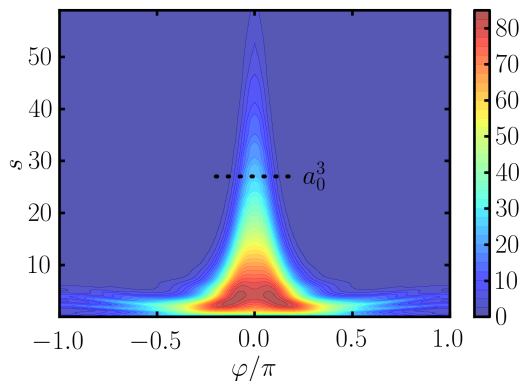


FIG. 4: Contour plot of the energy resolved spectrum  $dE/d\varphi ds$  over the  $\varphi$ - $s$  plane. The calculation is for  $N = 1$ ,  $a_0 = 3$  and  $\phi_{\text{CE}} = 0$ . The typical range of values of  $s$  is of the order of  $a_0^3$ .

of the vector potential, the value of  $a_0$ , which refers to the peak value of  $A^\mu$ , is relevant only in the direction where the maximum occurs, which is for  $\varphi = 0$  in our case. That means in the direction  $\varphi = 0$  high-energetic photons with large values of the variable  $s$  are emitted, while in the opposite direction,  $\varphi = \pi$ , only low-energy photons are emitted, see Fig. 4. Since we are considering here the emitted energy, the emission of high-energy photons with large values of the variable  $s$  is weighted stronger than it would be the case for

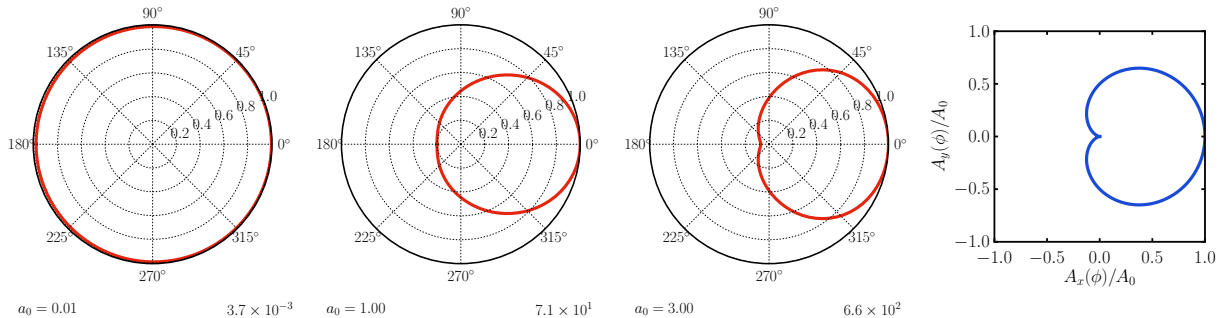


FIG. 5: Azimuthal energy emission spectra as in Fig. 3 but for circular laser polarization with  $\xi = \pi/4$ . In the rightmost panel, the values of the laser vector potential are plotted in the  $x$ - $y$  plane. The direction  $\varphi = 0$  is distinguished by the maximum of the vector potential.

the emission probability. Thus, the azimuthal distributions of the emitted energy  $dE/d\varphi$  are more sensitive to asymmetries of the vector potential than the corresponding azimuthal emission probabilities  $dW/d\varphi$ .

In Fig. 5, the azimuthal spectrum  $dE/d\varphi$  is exhibited in polar plots for a circularly polarized single-cycle ( $N = 1$ ) laser pulse with  $\xi = \pi/4$  and increasing values of  $a_0$  from left to right, showing the asymmetry in strong laser pulses. This is due to the fact that the vector potential has no azimuthal symmetry for an ultra-short pulse, since a distinguished direction is defined by the maximum of the laser pulse vector potential. As in the case of linear polarization, only in that direction where  $A^\mu$  reaches its maximum value, high frequency photons with large values of the variable  $s$  are emitted. The behaviour of the vector potential in the azimuthal plane is depicted in the rightmost panel of Fig. 5.

A weak short laser pulse with  $a_0 \ll 1$  does not show strong asymmetry effects. This asymmetry is a combined short-pulse intensity effect mainly due to the directional emission of high harmonics with  $s \gg 1$  (see Fig. 4). The transition from a distribution which is peaked perpendicularly to the laser polarization (see Fig. 3, left polar diagram) to a distribution peaked in the direction of the laser polarization vector (see Fig. 3, middle polar diagram) is characteristic for increasing the value of  $a_0$  below unity to larger than unity. The details of the shape of the distribution for  $a_0 > 1$ , i.e. whether one observes a dipole-type pattern or an uni-directional emission, depends on further pulse shape parameters. These dependencies are studied in the following.

Note that the photon distribution is determined by the shape and the symmetries of the

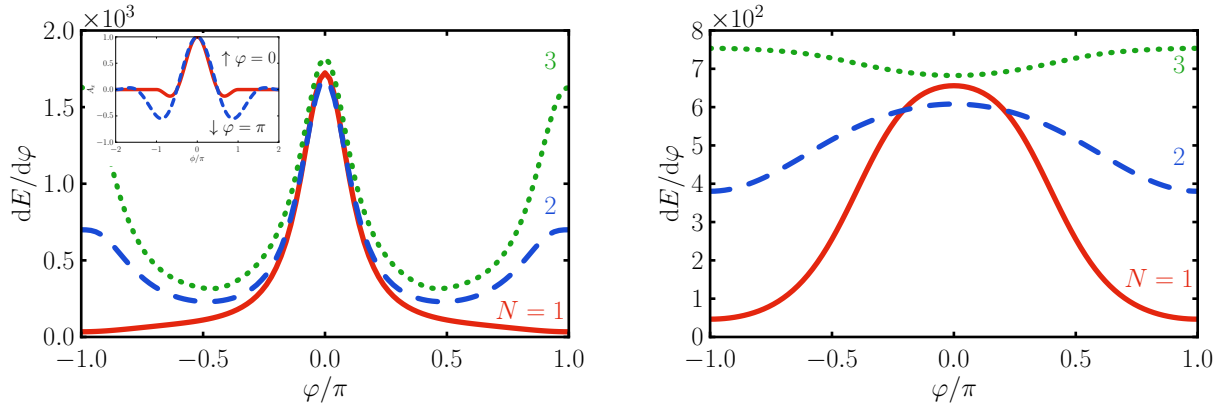


FIG. 6: Pulse length dependence of the azimuthal distributions  $dE/d\varphi$  for non-linear Compton scattering for linear (circular) polarization in the left (right) panel for  $a_0 = 3$  and  $\phi_{\text{CE}} = 0$ . The line styles represent  $N = 1$  (red solid), 2 (blue dashed), 3 (green dotted).

laser vector potential, and not by the electric field (see also the discussion in [38]), since the Volkov wave functions (3) as well as the classical electron velocity  $u^\mu$  in Eq. (A1) both depend directly on the laser vector potential  $A^\mu$ .

## 2. Dependence on the pulse length

The above discussion was for single-cycle laser pulses with various strengths. Here, we now present a systematic survey of the pulse length dependence of the azimuthal emission spectra for fixed values of  $a_0$ . For low laser intensity,  $a_0 \ll 1$ , the shape of the azimuthal distribution is independent of the pulse length  $N$ . On the contrary, in strong laser pulses the shape of the spectra strongly depends on the pulse length. While for  $N = 1$  the emission pattern in a strong laser pulse is highly asymmetric for a linearly polarized laser pulse, it is expected to become  $\pi$ -periodic for long pulses, with the limit being the result of an infinite plane wave, where the electron's quiver motion also becomes periodic. Increasing the pulse length from  $N = 1$  to 2 oscillations adds to the azimuthal spectrum only in the direction  $\varphi = \pi$ , since the vector potential at the center of the pulse, responsible for the emission in the direction  $\varphi = 0$ , remains almost unchanged, see left panel of Fig. 6.

Going further to  $N = 3$ , the results for the azimuthal spectra show a considerable restoration of that left-right symmetry. However, there is still a measurable difference of the order of

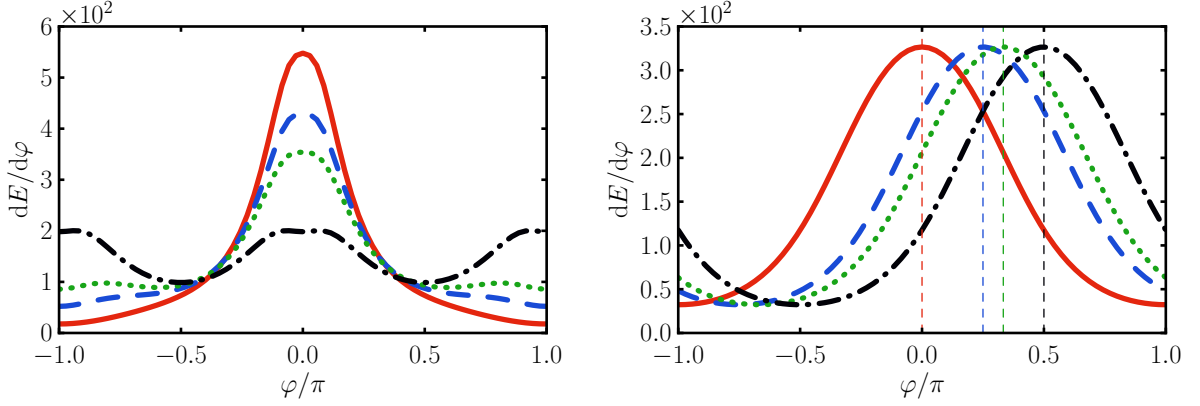


FIG. 7: Systematics of the dependence of azimuthal energy distribution  $dE/d\varphi$  on the CEP for linear polarization in the  $x$  direction ( $\xi = 0$ , left panel) and circular polarization ( $\xi = \pi/4$ , right panel). The different curves in each panel are for various values of the CEP:  $\phi_{CE} = 0$  (red solid curve),  $\pi/4$  (blue dashed),  $\pi/3$  (green dotted) and  $\pi/2$  (black dash-dotted). In all cases  $a_0 = 2$  and  $N = 1$ .

12%. For even longer pulses, the symmetry restoration proceeds further, such that for pulses longer than  $N = 5$  the differences are reduced to the level of below 1% and slowly decreases further for even longer pulses. Thus, for long pulses one observes a bi-polar emission pattern in the direction of the laser polarization.

Analogously, the strong azimuthal anisotropies must disappear for longer laser pulses in the case of circular laser polarization. For still rather short pulses with  $N = 3$  the azimuthal isotropy is recovered partly, see right panel of Fig. 6. Interestingly, the maximum of the spectrum for  $N = 1$  develops into the minimum for  $N = 3$ . For very long pulses one recovers azimuthal isotropy.

### 3. Dependence on the carrier envelope phase

At low laser intensity,  $a_0 \ll 1$ , the shape of the azimuthal distributions does not depend on the value of  $\phi_{CE}$ . However, for large values of  $a_0$ , there is a strong dependence of the azimuthal energy distribution on the CEP. For  $\phi_{CE} = 0$  the emission probability has the strong unidirectional characteristics with a maximum at  $\varphi = 0$ , since then the laser vector potential is strongly antisymmetric and large values are achieved only in the direction

$\varphi = 0$ . The shape of the spectrum changes upon increasing  $\phi_{\text{CE}}$  up to  $\phi_{\text{CE}} = \pi/2$  from the unidirectional emission to a bi-polar pattern for  $\phi_{\text{CE}} = \pi/2$  in the direction of the polarization three-vector  $\boldsymbol{\epsilon} = \mathbf{e}_x$  of the laser, see left panel of Fig. 7. In the case of  $\phi_{\text{CE}} = \pi/2$ , the laser vector potential is symmetric with respect to  $\varphi = 0$  and  $\varphi = \pi$  in the sense that the maximum value of the vector potential in the left and right hemispheres has the same value. This symmetry is translated to the left-right symmetry of the azimuthal spectrum. Upon increasing  $\phi_{\text{CE}}$  further up to  $\phi_{\text{CE}} = \pi$ , one finds an unidirectional emission with the maximum at  $\varphi = \pi$ , i.e. the opposite direction as for  $\phi_{\text{CE}} = \pi$ , reflecting the opposite sign of the vector potential in that case. This sensitive dependence on the CEP  $\phi_{\text{CE}}$  for  $a_0 \gtrsim 1$  is the basis for an experimental access to the CEP proposed in [11] for ultra-strong laser pulses, although it was discussed there in terms of the polar angle spectra.

In the case of circular laser polarization, the shape of the spectrum does not depend on the value of the CEP, but the position of the maximum of the distribution does. This is exhibited in the right panel of Fig. 7, where the different curves represent the azimuthal spectra for various values of  $\phi_{\text{CE}}$ . The straight vertical lines mark the maxima of the respective distributions and are equal to the value of the CEP. Although the usual azimuthal symmetry, which is a typical characteristic of a long circularly polarized laser pulse, is lost, a new symmetry arises. In a short laser pulse, the Compton spectrum depends only on the difference  $\varphi - \phi_{\text{CE}}$ , replacing the usual azimuthal symmetry. This effectively reduces one degree of freedom of the parameter space, since the coordinate system may always be oriented such that it corresponds to  $\phi_{\text{CE}} = 0$  in our parametrization of the laser pulse, i. e. the maximum of the vector potential occurs for  $\varphi = 0$ .

This symmetry can be deduced analytically from the expressions (17) for the differential emission probability. In general, any of the four functions  $\mathcal{C}_n$  entering  $w$  depends on the CEP through their non-linear phase factors  $f(\phi)$  (cf. Eq. (12)). Additional dependencies in the three functions  $\mathcal{C}_{\pm}$  and  $\mathcal{C}_2$  cancel from the expression (17) upon specifying circular polarization, i.e. for  $\cos 2\xi = 0$ . For the non-linear phase  $f(\phi)$  of the  $\mathcal{C}_n$  we find for head-on collisions (cf. Eq. (12)) that  $\varphi$  and  $\phi_{\text{CE}}$  appear solely in the combination

$$\epsilon_+ \cdot \mathbf{p}' e^{-i\phi_{\text{CE}}} = -\epsilon_+ \cdot \mathbf{k}' e^{-i\phi_{\text{CE}}} = \frac{\omega' \sin \vartheta}{\sqrt{2}} e^{\pm i(\varphi - \phi_{\text{CE}})} \quad (23)$$

proving that the differential probability  $w$  depends only on the difference  $\varphi - \phi_{\text{CE}}$  and not on the individual values of  $\varphi$  and  $\phi_{\text{CE}}$ .

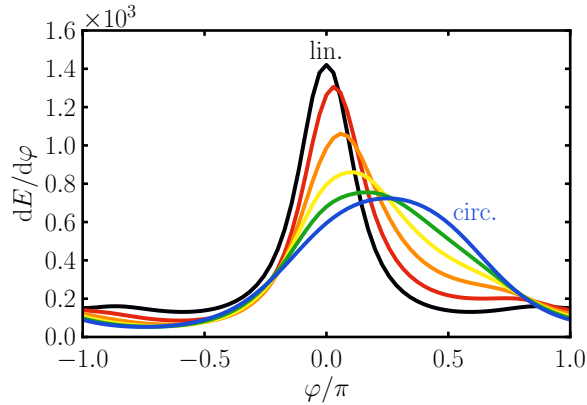


FIG. 8: Azimuthal emission spectra for  $a_0 = 3$ ,  $N = 1$ ,  $\phi_{\text{CE}} = \pi/4$  and various values of the laser polarization parameter starting with linear polarization  $\xi/\pi = 0$  (black curve, “lin.”) and increasing the value of  $\xi/\pi$  in steps of 0.05 up to  $\xi/\pi = 0.25$  corresponding to circular polarization (blue curve, “circ.”).

#### 4. Dependence on the laser polarization

Hitherto we considered the extreme cases of linear ( $\xi = 0$ ) and circular ( $\xi = \pi/4$ ) laser polarization. Now, the impact of intermediate elliptic polarizations on the azimuthal distributions is analysed. The azimuthal emission spectra for a single-cycle laser pulse,  $N = 1$ , are exhibited for  $a_0 = 3$  and  $\phi_{\text{CE}} = \pi/4$  in Fig. 8 for various laser polarizations  $\xi$  ranging from linear over elliptic to circular polarization. Indeed, the azimuthal emission spectra show a characteristic dependence on the polarization of the laser pulse, which gradually develops from the narrow unidirectional emission on the axis of polarization for linear polarization (black curve in Fig. 8) to the directional emission into the preferential direction  $\varphi = \phi_{\text{CE}} = \pi/4$  for circular polarization (blue curve in Fig. 8). The peak position of the distribution is shifted monotonically to the right with increasing value of  $\xi$  and the shape of the distribution gradually changes. For generically elliptic laser polarization, the azimuthal distributions are very asymmetric.



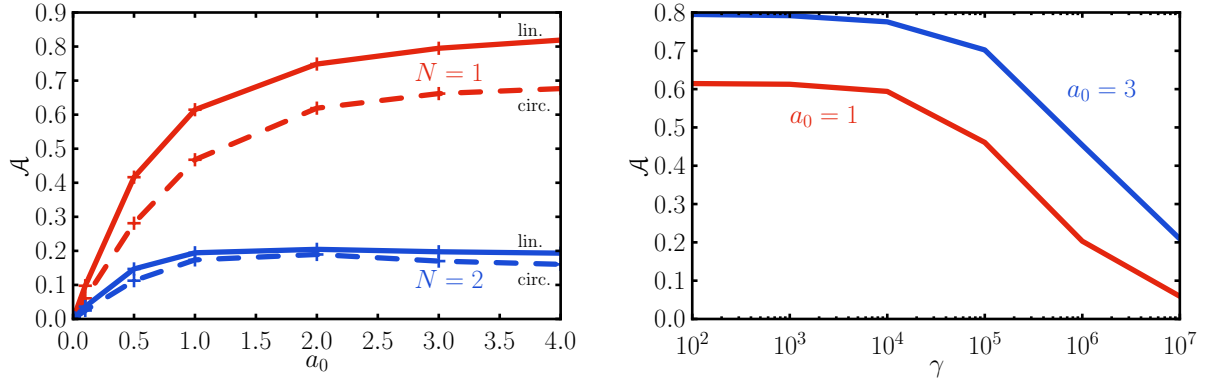


FIG. 9: Left panel: The azimuthal asymmetry  $\mathcal{A}$  as a function of the laser strength  $a_0$  for a single-cycle pulse ( $N = 1$ ) and a two cycle pulse ( $N = 2$ ) for  $\gamma = 100$ . Solid (dashed) curves are for linear (circular) polarization. Right panel: Anisotropy  $\mathcal{A}$  as a function of the initial electron energy  $\gamma$  for  $a_0 = 1$  (lower red curve) and  $a_0 = 3$  (upper blue curve) and linear polarization.

### C. Asymmetries of the azimuthal distributions

The differential information in the azimuthal distribution  $dE/d\varphi$  may be further condensed in the asymmetry  $\mathcal{A}$  defined as

$$\mathcal{A} = \frac{E_{\rightarrow} - E_{\leftarrow}}{E_{\rightarrow} + E_{\leftarrow}}, \quad (24)$$

where

$$E_{\rightarrow}^{\text{lin}} = \int_{-\frac{\pi}{2}}^{\frac{\pi}{2}} d\varphi \frac{dE}{d\varphi}, \quad E_{\leftarrow}^{\text{lin}} = \int_{\frac{\pi}{2}}^{\frac{3\pi}{2}} d\varphi \frac{dE}{d\varphi} \quad (25)$$

denotes the energy emitted into the right ( $\rightarrow$ ) and left ( $\leftarrow$ ) hemispheres, respectively, for linear polarization. For circular polarization, we exploit the symmetry in the variable  $\varphi - \phi_{\text{CE}}$

$$E_{\rightarrow}^{\text{circ}} = \int_{-\frac{\pi}{2} + \phi_{\text{CE}}}^{\frac{\pi}{2} + \phi_{\text{CE}}} d\varphi \frac{dE}{d\varphi}, \quad E_{\leftarrow}^{\text{circ}} = \int_{\frac{\pi}{2} + \phi_{\text{CE}}}^{\frac{3\pi}{2} + \phi_{\text{CE}}} d\varphi \frac{dE}{d\varphi} \quad (26)$$

by shifting the orientation of the hemispheres by the value of the CEP. Results for the asymmetry  $\mathcal{A}$  as a function of  $a_0$  are exhibited in Fig. 9 (left panel). We use  $\phi_{\text{CE}} = 0$  which provides the largest values of  $\mathcal{A}$ . From the results in Fig. 9 it becomes clear that a large asymmetry is possible only for short pulses, e.g. for  $N = 1$ , where linear polarization

provides larger asymmetries than circular polarization. Increasing the pulse length to  $N = 2$  leads to a reduction of the asymmetry, e.g. for  $a_0 = 4$  and linear polarization  $\mathcal{A}$  drops from 0.82 to 0.19.

Within the classical theory of Thomson scattering based on electron trajectories, which we briefly discuss in Appendix A, the shape of the angular Compton spectrum depends only on the ratio  $a_0/\gamma$  but not on the individual values  $a_0$  and  $\gamma$  [39]. This scaling behaviour is violated within a quantum theoretical framework due to the electron recoil. For increasing centre-of-mass energies,  $\mathfrak{s} = (k + p)^2 \gg m^2$ , the anisotropies are gradually reduced until one finds an isotropic emission pattern despite of the linear polarization of the laser field. In Compton backscattering of optical photons, a higher centre-of-mass energy is related to a larger value of the electron Lorentz factor  $\gamma$  by means of  $\mathfrak{s} \simeq m^2(1 + 4\gamma^2\omega/m)$ . In the right panel of Fig. 9, the degradation of the asymmetry with increasing values of  $\gamma$  is exhibited. For instance, for a high-energy electron beam with  $\gamma = 10^5$ , which were used in the SLAC E-144 experiment [9], the asymmetry has a value of 0.46 for  $a_0 = 1$  as compared to 0.61 for the previously discussed low-energy regime with  $\gamma = 100$  accessible, e.g. at the HZDR.

A similar reduced dependence on the azimuthal angle for high centre-of-mass energies is also found in perturbative QED [40]. The corresponding expression for the emission cross section of a polarized photon is presented in Appendix B. As shown in Eq. (B6), the leading order in the ultra-relativistic limit  $\mathfrak{s} \gg m^2$  is independent of the azimuthal angle  $\varphi$ . The qualitative arguments that explain this behaviour are as follows: For  $\mathfrak{s} \gg m^2$ , the centre-of-mass frame, in which the momenta of the outgoing electron and photon are back-to-back, moves rapidly with respect to both the laboratory frame and the frame where the electron is initially at rest. Transforming back from the centre-of-mass frame the scattering angle of the emitted photon is boosted close to the forward scattering direction to values  $\vartheta \simeq \pi - \gamma^{-1}$ . Close to forward scattering the coefficients of the non-linear phase integrals are of the order  $\alpha_+ = \mathcal{O}(a_0/\gamma)$  and  $\beta = \mathcal{O}(a_0^2/\gamma^2)$ , i.e. both are small compared to unity. Thus, the emission of high frequency photons with large values of the variable  $s$ , which are responsible for the asymmetries in the azimuthal emission patterns, are strongly suppressed.

#### IV. TOTAL EMITTED ENERGY

After having characterized the angular distribution of the energy integrated photon intensity, we now briefly discuss the total amount of energy  $E$  which is radiated off in the non-linear Compton process. For the situation considered here, characterized by  $a_0 \ll \gamma$ , we find  $E^{\text{cl}} = 2\gamma^2\sigma_T\Phi$  within a classical framework for the emission of radiation (i.e. Thomson scattering, see Appendix A). The quantity  $\sigma_T = 665$  mb denotes the Thomson cross section, which is related to the classical electron radius  $r_e$  via  $\sigma_T = 8\pi r_e^2/3$ , and  $\Phi = \int dx^+ n_i T^{i0}(\phi)$  is the primary energy flux, integrated over the light-front time  $x^+$  with  $n_i$  denoting the spatial components of the laser propagation direction. The integrated primary energy flux  $\Phi$  corresponds to the total laser energy irradiated onto a unit area during a single pulse. For the laser vector potential  $A^\mu$  given in (2), we find the energy momentum tensor  $T^{\mu\nu} = -k^\mu k^\nu A' \cdot A'$ . (The prime denotes the derivative w.r.t. the laser phase  $\phi$ .) Evaluating the derivative, the integrated energy flux can be written as  $\Phi = \frac{m^2 a_0^2 \omega}{2e^2} \Delta\phi_{\text{eff}}$  with the effective pulse length  $\Delta\phi_{\text{eff}} = \int_{-\infty}^{\infty} d\phi [(g^2 + g'^2) - \cos 2\xi \{(g^2 - g'^2) \cos 2(\phi + \phi_{\text{CE}}) + 2g'g \sin 2(\phi + \phi_{\text{CE}})\}]$ . For longer pulses ( $N > 5$ ) it is suitable to approximate the integrand as  $g^2(\phi)$ , such that we find  $\Delta\phi_{\text{eff}} \simeq 3\pi N/4$  for the specific pulse shape (20).

The emitted energy  $E$  is exhibited in Fig. 10 as a function of  $\gamma$  for  $a_0 = 0.1, 1$  and  $3$  from bottom to top. For increasing values of  $\gamma$ , the total emitted energy stays below the classical value  $E^{\text{cl}}$ , which is a quantum effect due to the electron recoil. The deviations start to become relevant for  $\gamma$  between  $10^3$  and  $10^4$ . It is found that for higher laser intensity, the full quantum calculation deviates from the classical expression already for lower values of  $\gamma$ . This is due to the emission of high harmonics with large values of the variable  $s$  in that case. The relevant recoil parameter is  $s\omega/m$ , which may be large even if one is still in the low-energy regime, characterized by  $\omega/m \ll 1$ . This is in line with recently published results [41] on the total emitted energy for ultra-high laser intensity.

The total emitted energy is insensitive to the shape of the pulse. The relevant quantity is the integrated flux of energy in the laser pulse  $\Phi \propto a_0^2 N$ . This in contrast to the cross channel process of Breit-Wheeler type pair production, where a strong enhancement of the emission probability in ultra-short laser pulses was found near the threshold region [42, 43].

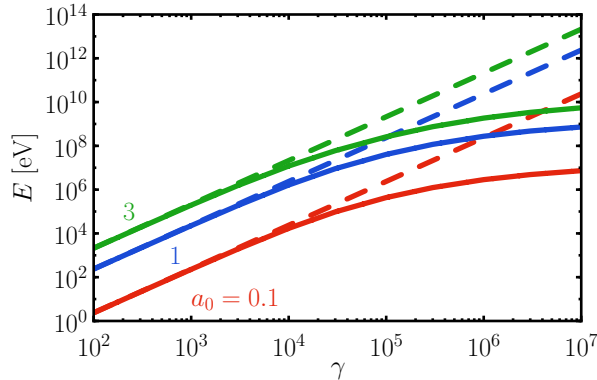


FIG. 10: Total emitted energy  $E$  as a function of  $\gamma$  for various values of  $a_0 = 0.1$  (lower red curves), 1 (middle blue curves) and 3 (upper green curves). The solid curves depict the full quantum result while the dashed curves refer to the classical approximation  $E^{\text{cl}}$ .

## V. DISCUSSION AND SUMMARY

We study Compton backscattering of an ultra-short intense laser pulse off an electron beam. Non-linear and multi-photon effects are accounted for by working in the Furry picture with laser dressed Volkov states. Compton backscattering of a laser beam off an electron beam is interesting with respect to the development of compact broadband pulsed X-ray radiation sources, as outlined in the Introduction. A prerequisite of technical design studies is a comprehensive understanding of the elementary process. To characterize the back-scattering spectrum we analyse angular distributions which provide a clear signal of non-linear effects and show novel signatures in ultra-short pulses. The angular distributions have the advantage not to be hampered by detector pile-ups as they represent an energy integrated distribution which is experimentally accessible in a calorimetric measurement.

It is shown that the energy integrated azimuthal spectra show a strong dependence on both the laser polarization and the value of the carrier envelope phase for ultra-short laser pulses. The asymmetry for circular polarization is explained by the preferred direction where the vector potential reaches its maximum value which breaks the usual azimuthal symmetry. The azimuthal distribution displays a symmetry with respect to the difference of the azimuthal angle and the carrier envelope phase for ultra-short circularly polarized laser pulses. This replaces the general azimuthal symmetry of infinitely long circularly polarized plane waves.

For non-phase-locked lasers one needs to perform single-shot measurements in order to see the asymmetries in the azimuthal spectra. For an electron bunch charge of 77 pC with gamma factor  $\gamma = 100$  interacting with a single-cycle laser pulse with intensity  $2 \times 10^{18} \text{W/cm}^2$ , we estimate the total number of photons as  $2.8 \times 10^6$  with a total amount of deposited energy of 18 nJ in the detector. This assumes an optimal overlap of the laser pulse and the electron bunch.

The total emitted energy is proportional to the integrated primary energy flux in the laser pulse in the low-energy regime and scales with the square of the primary electron energy within a classical framework. At high laser intensity we see deviations from the classical scaling behaviour even in the Thomson regime due to the emission of high harmonics, for which the quantum recoil is relevant. The low-energy Thomson regime is representative for head-on collisions of optical laser beams and mildly relativistic electron beams. For instance, the DRACO-ELBE constellation at the HZDR fulfils this requirement. Although the asymmetries for single-cycle pulses are presently out of reach of the DRACO-ELBE system due to long laser pulses, the transition from perpendicular emission for low laser intensity to parallel emission with respect to the laser polarization for high intensity could well be tested experimentally as a clear signal for non-linear effects in Compton scattering. Our calculations apply for a section of transverse laser beam profile where the curvature of the wave fronts is negligible since we rely on a plane wave approximation. We restrict our analysis to mildly intense laser pulses with intensity of the order of  $10^{19} \text{W/cm}^2$  which can be achieved in rather large laser spots with sub-PW lasers, such that the effects of the curvature of the laser fronts is negligible. Multi-photon emission, e.g. via the two-photon Compton process [35], is expected to provide only a minor contribution to the radiation spectrum.

Focusing on the azimuthal distribution means considering the energy and polar angle integrated spectra. In particular, the pile-ups prevent in present-day detector technology the easy measurement of energy-differential spectra for large incident photon fluxes, even if they are interesting with respect to harmonics and their substructures. The energy integrated quantities  $dE/d\Omega$  and  $dE/d\varphi$  are, in contrast, easily accessible experimentally since they require an angularly resolved calorimetric measurement of the energy distributions.

We mention that all numerical results presented are for a particular temporal laser pulse shape. It is straightforward to replace the employed function by other, possibly multi-

parameter envelopes.

In summary we consider the non-linear Compton process of mildly relativistic electrons interacting with medium-intense short and ultra-short laser pulses. As a key to the radiation spectrum we propose the angular distributions which are free of the notorious problem of pile-ups which may be faced in energy differential spectra and provide clear signals of non-linear Compton scattering. The impact of the laser intensity, the pulse length and the carrier envelope phase on the energy-integrated azimuthal distributions is studied systematically. Measurements of the azimuthal and polar angle distributions may serve as useful tool to quantify both the electron beam and the laser beam parameters.

The parameter space which we have considered is representative for many lasers worldwide in the sub-PW regime, i.e. for intensity parameters  $a_0 < 10$ . The ultra-intense regime deserves separate investigations. In contrast, our consideration of ultra-short pulses with essentially one oscillation of the electromagnetic field in a pulse is at the limit of present-day technological feasibility. The peculiarities, such as the strong asymmetry of the azimuthal distribution for circularly polarized laser radiation or the strong one-side asymmetry for linearly polarized laser radiation, disappears quickly for more oscillations of the electromagnetic field. Therefore, such measures are particularly suitable tools for the characterization ultra-short pulses.

## Acknowledgments

The authors thank A. I. Titov, T. Heinzl, A. Otto, T. Nusch and T. E. Cowan for continuous useful discussions and collaboration. The support by R. Sauerbrey, T. Stöhlker and S. Fritzsche is gratefully acknowledged. G. Paulus pointed out the important role of the carrier envelope phase which we subsequently considered here.

## Appendix A: Classical Radiation: Thomson Scattering

In the classical picture, which is valid if the electron recoil during the interaction is negligible [26], an ultra-relativistic electron, moving in an external electromagnetic wave field, emits radiation only into directions which are swept by the instantaneous tangent vector to its trajectory, i.e. the spatial part  $\mathbf{u}$  of the four-velocity  $u^\mu(\tau) = dx^\mu/d\tau = (\gamma, \mathbf{u})$ , with proper

time  $\tau$ . For plane wave laser fields, the orbit reads in terms of the laser vector potential  $A^\mu$

$$u^\mu(\tau) = u_0^\mu - \frac{e}{m} A^\mu + k^\mu \left( \frac{e}{m} \frac{u_0 \cdot A}{k \cdot u_0} - \frac{e^2}{m^2} \frac{A \cdot A}{2k \cdot u_0} \right). \quad (\text{A1})$$

The differential radiated power of an electron moving on an arbitrary trajectory reads (cf. [44], Eq. (14.37))

$$\frac{dE(t')}{d\Omega dt'} = \frac{\alpha}{4\pi} \left. \frac{|\mathbf{n}' \times [(\mathbf{n}' - \mathbf{v}) \times \frac{d\mathbf{v}}{dt}]|^2}{(1 - \mathbf{n}' \cdot \mathbf{v})^6} \right|_{\text{ret}}. \quad (\text{A2})$$

Integration over observation time  $t'$  and a change of the integration variables retarded time  $t$  yields

$$\frac{dE}{d\Omega} = \frac{\alpha}{4\pi} \int dt \frac{|\mathbf{n}' \times [(\mathbf{n}' - \mathbf{v}) \times \frac{d\mathbf{v}}{dt}]|^2}{(1 - \mathbf{n}' \cdot \mathbf{v})^5}. \quad (\text{A3})$$

Now, we replace the velocity  $\mathbf{v} = d\mathbf{x}/dt$  by the four-velocity  $u^\mu$  and change the integration variable from  $t$  to the laser phase  $\phi$  via  $dt = \frac{dt}{d\tau} \frac{d\tau}{d\phi} d\phi = \frac{\gamma}{k \cdot u_0} d\phi$ . We have  $\mathbf{v} = \mathbf{u}/\gamma$  and  $d\mathbf{v}/dt = (\dot{\mathbf{u}}\gamma - \mathbf{u}\dot{\gamma})/\gamma^3$ , where the dot denotes the derivative w.r.t. proper time  $\tau$ . Using these relations we obtain

$$\frac{dE}{d\Omega} = \frac{\alpha}{4\pi k \cdot u_0} \int d\phi \frac{|\mathbf{n}' \times [(\mathbf{n}'\gamma - \mathbf{u}) \times (\dot{\mathbf{u}}\gamma - \mathbf{u}\dot{\gamma})]|^2}{\gamma^2 (n' \cdot u)^5}. \quad (\text{A4})$$

The evaluation of the square of the double cross product yields, exploiting the relativistic constraints  $u \cdot u = 1$  and  $\dot{u} \cdot u = 0$ , the result

$$\begin{aligned} \frac{1}{\gamma^2} |\mathbf{n}' \times [(\mathbf{n}'\gamma - \mathbf{u}) \times (\dot{\mathbf{u}}\gamma - \mathbf{u}\dot{\gamma})]|^2 &= -(n' \cdot \dot{u})^2 - (n' \cdot u)^2 \dot{u}^2 \\ &= - \left( \frac{d}{d\tau} n' \cdot u u^\mu \right)^2. \end{aligned} \quad (\text{A5})$$

Thus, the radiated energy is given by the expression

$$\frac{dE}{d\Omega} = - \frac{\alpha k \cdot u_0}{4\pi} \int \frac{d\phi}{(n' \cdot u)^5} \left( \frac{d}{d\phi} n' \cdot u u^\mu \right)^2. \quad (\text{A6})$$

Using the trajectory as a function of the laser vector potential in Eq. (A1) allows to calculate the angular radiation spectrum. Our result (A6) compares well to the result in [39]. However, we provide a covariant expression in terms of the orbit  $u^\mu$  in a plane wave (A1) and furthermore, we do not rely on the approximation  $\mathbf{u} \parallel \mathbf{n}'$  to simplify the expression for the emitted energy distribution.

To calculate the total amount of radiated energy we may either integrate (A6) over the full solid angle or alternatively use the Larmor formula for the emitted power (cf. [44], Eq. (14.24))

$$\frac{dE^{\text{cl}}}{dt} = -\frac{1}{6\pi} \frac{e^2}{m^2} \dot{p} \cdot \dot{p}. \quad (\text{A7})$$

With the classical equations of motion for the electron  $\dot{p}^\mu = \frac{e}{m} F^{\mu\nu} p_\nu$ , where  $F_{\mu\nu} = \partial_\mu A_\nu - \partial_\nu A_\mu$  is the electromagnetic field strength tensor of the laser field, the emitted power can be expressed as

$$\frac{dE^{\text{cl}}}{dt} = \frac{1}{6\pi} \frac{e^4}{m^4} p_\mu F^{\mu\nu} F_\nu{}^\kappa p_\kappa = \frac{1}{6\pi} \frac{e^4}{m^4} p_\mu T^{\mu\nu} p_\nu, \quad (\text{A8})$$

where the last step is valid for a null background field, as is used here. Evaluating the energy momentum tensor for the vector potential (2) one finds  $T^{\mu\nu} = k^\mu k^\nu T^{00}/\omega^2$ . Thus, the emitted power is proportional to the energy density of the background field

$$\frac{dE^{\text{cl}}}{dt} = \frac{1}{6\pi} \frac{e^4 (k \cdot p)^2}{m^4 \omega^2} T^{00}. \quad (\text{A9})$$

The total energy emitted in such a process is the coordinate time integral of (A9), which needs to be transformed into an integral over the laser phase as above, yielding

$$E^{\text{cl}} = \frac{8}{3} \pi r_e^2 \frac{k \cdot u_0}{\omega^2} \int d\phi \gamma(\phi) T^{00}(\phi). \quad (\text{A10})$$

For head-on collisions with  $\gamma_0 \gg 1$ , one finds  $\gamma(\phi) \simeq \gamma_0 [1 + \mathcal{O}(a_0/\gamma_0)^2]$  indicating that for moderately intense lasers with  $a_0 \ll \gamma_0$ , the initial value  $\gamma^0$  is the leading-order contribution which can be taken out of the integral. Thus, the emitted energy is proportional to the integrated energy flux of the laser pulse  $\Phi$ , and  $E^{\text{cl}} \simeq 2\gamma_0^2 \sigma_T \Phi$ . The next-to-leading order gives a positive correction, whereas the quantum corrections, that scale with the quantum non-linearity parameter  $\chi$ , have a negative sign [32].

## Appendix B: Perturbative Compton Scattering with Linearly Polarized Photons

In perturbative QED, the cross section for Compton scattering of unpolarized electrons and polarized photons reads in the rest frame of the incoming electron [40]

$$\frac{d\sigma}{d\Omega} = \frac{r_e^2}{4} \left( \frac{\omega'}{\omega} \right)^2 \left( \frac{\omega'}{\omega} + \frac{\omega}{\omega'} - 2 + 4(\boldsymbol{\epsilon} \cdot \boldsymbol{\epsilon}')^2 \right), \quad (\text{B1})$$



where  $\epsilon$  ( $\epsilon'$ ) denotes the polarization vector of the incoming (outgoing) photon and

$$\omega' = \frac{\omega}{1 + \nu(1 + \cos \vartheta)} \quad (\text{B2})$$

is the frequency of the outgoing photon as a function of the scattering angle  $\vartheta$  (note that in our convention forward scattering is denoted by  $\vartheta = \pi$ );  $r_e = \alpha/m$  is the classical electron radius and  $\nu = \omega/m$  denotes normalized laser frequency such that the centre-of-mass energy squared is  $\mathfrak{s} = m^2(1+2\nu)$ . Specifying  $\epsilon = e_x$  and summing over the final photon polarizations we obtain

$$\frac{d\sigma}{d\Omega} = \frac{r_e^2}{2} \left( \frac{\omega'}{\omega} \right)^2 \left( \frac{\omega'}{\omega} + \frac{\omega}{\omega'} - 2 \cos^2 \varphi \sin^2 \vartheta \right). \quad (\text{B3})$$

The integration over the polar angle  $\vartheta$  yields the azimuthal distribution

$$\frac{d\sigma}{d\varphi} = \frac{r_e^2}{2} \left( \frac{\log(1+2\nu)}{\nu} + 2 \frac{(1+\nu)}{(1+2\nu)^2} - \frac{4 \cos^2 \varphi}{\nu^3} [(1+\nu) \log(1+2\nu) - 2\nu] \right). \quad (\text{B4})$$

The non-relativistic ( $\nu \ll 1$ ) and ultra-relativistic ( $\nu \gg 1$ ) limits read

$$\frac{d\sigma}{d\varphi} = \frac{r_e^2}{2} \left[ \left( 4 - \frac{8}{3} \cos^2 \varphi \right) - 2\nu \left( 4 - \frac{8}{3} \cos^2 \varphi \right) \right] + \mathcal{O}(\nu^2), \quad \nu \ll 1 \quad (\text{B5})$$

$$\frac{d\sigma}{d\varphi} = \frac{r_e^2}{2} \left[ \frac{1}{\nu} \left( \frac{1}{2} + \log 2\nu \right) + \frac{1}{\nu^2} \left( \frac{1}{2} + 8 \cos^2 \varphi - 4 \cos^2 \varphi \log 2\nu \right) \right] + \mathcal{O}(\nu^{-3}), \quad \nu \gg 1. \quad (\text{B6})$$

The leading-order term of the non-relativistic limit of the perturbative cross section gives the same azimuthal distribution as in the general expression  $dW/d\varphi$  (or  $dE/d\varphi$ ) for weak short laser pulses, i.e. in the limit  $a_0 \ll 1$ . On the contrary, the leading order of the ultra-relativistic limit turns out to be independent of the azimuthal angle  $\varphi$ ; an azimuthal dependence enters first at next-to-leading order.

- 
- [1] M. Carpinelli and L. Serafini (eds.), “Compton sources for X/γ rays: Physics and applications” Nucl. Instr. Meth. A **608** 1S (2009) .
- [2] A. Debus, M. Bussmann, M. Siebold, A. Jochmann, U. Schramm, T. Cowan, and R. Sauerbrey, Appl. Phys. B **100**, 61 (2010).
- [3] A. Di Piazza, C. Müller, K. Z. Hatsagortsyan, and C. H. Keitel, Rev. Mod. Phys. **84**, 1177 (2012).

- [4] A. R. Bell and J. G. Kirk, *Phys. Rev. Lett.* **101**, 200403 (2008).
- [5] A. M. Fedotov, N. B. Narozhny, G. Mourou, and G. Korn, *Phys. Rev. Lett.* **105**, 080402 (2010).
- [6] S.-Y. Chen, A. Maksimchuk, and D. Umstadter, *Nature* **396**, 653 (1998).
- [7] M. Babzien, I. Ben-Zvi, K. Kusche, I. V. Pavlishin, I. V. Pogorelsky, D. P. Siddons, V. Yakimenko, D. Cline, F. Zhou, T. Hirose, Y. Kamiya, T. Kumita, T. Omori, J. Urakawa, and K. Yokoya, *Phys. Rev. Lett.* **96**, 054802 (2006).
- [8] C. Bula, K. T. McDonald, E. J. Prebys, C. Bamber, S. Boege, T. Kotseroglou, A. C. Melissinos, D. D. Meyerhofer, W. Ragg, D. L. Burke, R. C. Field, G. Horton-Smith, A. C. Odian, J. E. Spencer, D. Walz, S. C. Berridge, W. M. Bugg, K. Shmakov, and A. W. Weidemann, *Phys. Rev. Lett.* **76**, 3116 (1996).
- [9] C. Bamber, S. J. Boege, T. Koffas, T. Kotseroglou, A. C. Melissinos, D. D. Meyerhofer, D. A. Reis, W. Ragg, C. Bula, K. T. McDonald, E. J. Prebys, D. L. Burke, R. C. Field, G. Horton-Smith, J. E. Spencer, D. Walz, S. C. Berridge, W. M. Bugg, K. Shmakov, and A. W. Weidemann, *Phys. Rev. D* **60**, 092004 (1999).
- [10] O. Har-Shemesh and A. Di Piazza, *Opt. Lett.* **37**, 1352 (2012).
- [11] F. Mackenroth, A. Di Piazza, and C. H. Keitel, *Phys. Rev. Lett.* **105**, 063903 (2010).
- [12] W. P. Leemans, R. W. Schoenlein, P. Volfbeyn, A. H. Chin, T. E. Glover, P. Balling, M. Zolotarev, K. J. Kim, S. Chattopadhyay, and C. V. Shank, *Phys. Rev. Lett.* **77**, 4182 (1996).
- [13] A. I. Nikishov and V. I. Ritus, *Sov. Phys. J. Exp. Theor. Phys.* **19**, 529 (1964).
- [14] A. I. Nikishov and V. I. Ritus, *Sov. Phys. J. Exp. Theor. Phys.* **19**, 1191 (1964).
- [15] A. I. Nikishov and V. I. Ritus, *Sov. Phys. J. Exp. Theor. Phys.* **20**, 757 (1965).
- [16] N. B. Narozhnyi, A. I. Nikishov, and V. I. Ritus, *Sov. Phys. J. Exp. Theor. Phys.* **20**, 622 (1965).
- [17] I. I. Goldman, *Phys. Lett.* **8**, 103 (1964).
- [18] L. S. Brown and T. W. B. Kibble, *Phys. Rev.* **133**, A705 (1964).
- [19] T. W. B. Kibble, *Phys. Rev.* **138**, B740 (1965).
- [20] C. Harvey, T. Heinzl, and A. Ilderton, *Phys. Rev. A* **79**, 063407 (2009).
- [21] F. Ehlotzky, K. Krajewska, and J. Z. Kamiński, *Rep. Prog. Phys.* **72**, 046401 (2009).
- [22] <http://extreme-light-infrastructure.eu>.
- [23] Z. Major, S. Klingebiel, C. Skrobol, I. Ahmad, C. Wandt, S. A. Trushin, F. Krausz, and

- S. Karsch, AIP Conf. Proc. **1228**, 117 (2010).
- [24] N. B. Narozhnyi and M. S. Fofanov, J. Exp. Theor. Phys. **83**, 14 (1996).
- [25] M. Boca and V. Florescu, Phys. Rev. A **80**, 053403 (2009), [Erratum in Phys. Rev. A **81**, 039901(E) (2010)].
- [26] D. Seipt and B. Kämpfer, Phys. Rev. A **83**, 022101 (2011).
- [27] F. Mackenroth and A. Di Piazza, Phys. Rev. A **83**, 032106 (2011), arXiv:1010.6251 hep-ph .
- [28] M. Boca and V. Florescu, Eur. Phys. J. D **61**, 449 (2011).
- [29] P. Lan, P. Lu, W. Cao, and X. Wang, J. Phys. B **40**, 403 (2007).
- [30] K. Krajewska and J. Z. Kamiński, Phys. Rev. A **85**, 062102 (2012).
- [31] D. M. Volkov, Z. Phys. **94**, 250 (1935).
- [32] V. I. Ritus, J. Sov. Laser Res. **6**, 497 (1985).
- [33] H. Mitter, Acta Physica Austriaca, Suppl. XIV , 397 (1975).
- [34] A. Ilderton, Phys. Rev. Lett. **106**, 020404 (2011), arxiv:1011.4072 .
- [35] D. Seipt and B. Kämpfer, Phys. Rev. D **85**, 101701 (2012).
- [36] F. Gabriel, P. Gippner, E. Grosse, D. Janssen, P. Michel, H. Prade, A. Schamlott, W. Seidel, A. Wolf, and R. Wünsch, Nucl. Instr. Meth. B **161-163**, 1143 (2000).
- [37] K. Zeil, S. D. Kraft, S. Bock, M. Bussmann, T. E. Cowan, T. Kluge, J. Metzkes, T. Richter, R. Sauerbrey, and U. Schramm, New J. Phys. **12**, 045015 (2010).
- [38] K. Krajewska and J. Z. Kamiński, Phys. Rev. A **86**, 021402 (2012), arXiv: 1204.3762 [hep-ph].
- [39] M. Boca and A. Oprea, Phys. Scr. **83**, 055404 (2011).
- [40] J. M. Jauch and F. Rohrlich, *The Theory of Photons and Electrons* (Springer-Verlag, Berlin, Heidelberg, New York, 1976).
- [41] V. Dimu, “Exact final state integrals for strong field QED,” (2013), arXiv:1302.1513 [hep-ph].
- [42] A. I. Titov, H. Takabe, B. Kämpfer, and A. Hosaka, Phys. Rev. Lett. **108**, 240406 (2012).
- [43] T. Nousch, D. Seipt, B. Kämpfer, and A. I. Titov, Phys. Lett. B **715**, 246 (2012).
- [44] J. D. Jackson, *Klassische Elektrodynamik*, 2nd ed. (Walter de Gruyter, Berlin, New York, 1983).